ON THE GAUSSIANITY VALIDITY TIME FOR ORBITAL UNCERTAINTY PROPAGATION

C. Yanez, M. Gupta, V. Morand, and J. C. Dolado

CNES, 18 av. Edouard Belin, 31401 Toulouse Cedex 9, France, Email: carlos.yanez@cnes.fr

ABSTRACT

Most of the algorithms and methods used in the field of Space Surveillance and Tracking (SST) assume that the orbital uncertainty of space objects is accurately described by a multivariate Gaussian (normal) distribution. However, it is well-known that being the space dynamics highly non-linear (especially in a Cartesian representation of the orbital state vector), the normal distribution assumption does not hold for a *long time* in the absence of new information/measurements.
This paper aims to quantify this *long time* by means of Multivariate Normal (MVN) statistical tests applied to Monte Carlo simulations. Moreover, an analytical method is proposed for determining the departure from Gaussianity that consists in monitoring the distance between the uncertainty distribution propagated by linear and non-linear techniques. Monte Carlo and analytical approaches are compared showing a good agreement. This provides an efficient method to assess the Gaussianity validity time of the propagation of orbital uncertainties.
A direct application of this method is to use the Gaussianity validity time as a threshold in the splitting criterion for a Gaussian Mixture Model representation.

Keywords: Gaussian distribution; Gaussianity breakdown; statistical tests; State Transition Tensor; Gaussian mixture models; uncertainty propagation.

1. INTRODUCTION

Space Surveillance and Tracking (SST) aims to study and monitor resident space objects (RSO) and maintain the information about them within a catalogue. This includes the detection, tracking, cataloguing and identification of RSO, along with the analysis of the resulting catalogue for providing services such as collision risk assessment and reentry predictions. In many of the aspects of SST, the accuracy and realism of the object state uncertainty play an essential role. Measurements data association, performance of sensor tasking, correct estimation of probability of collision, to name a few examples, would fail or degrade severely if the orbital uncertainty is inaccurately represented.
The general assumption is that this state uncertainty can be represented by a multi-variate normal (MVN) distribution. However, in the frame of SST, the scarce of measurements due to a great number of space objects to track and the limited sensor resources leads to the necessity of propagating the uncertainty during long periods of time (several orbital periods). The intrinsic non-linear dynamics of space objects along with long propagation times yield to the breakdown of the Gaussianity assumption, and, therefore, a single MVN is no longer a valid representation of the probability density function (PDF) of object state.
This work examines the validity time of the MVN representation in a twofold manner. Firstly, the use of statistical tests to evaluate the departure from MVN assumption of the uncertainty distribution in Monte Carlo (MC) simulations. The importance of the coordinates system for preserving the Gaussianity is evaluated with statistical tests, comparing the results when a Cartesian or Equinoctial representation of the orbital state vector is employed. Secondly, the effect of non-linearity is assessed by the comparison of orbital PDFs propagated with linear and non-linear methods. The measure of distance between both PDFs is evaluated with the scale-invariant Hellinger distance [19]. Linear propagation is performed with the usual State Transition Matrix (STM), whether the non-linear propagation makes use of higher order terms of the Taylor series linearization in the form of a State Transition Tensor (STT).
Both procedures are combined in order to link the departure from MVN representation to the importance of non-linear effects in the dynamics. Hence, it is possible to define a threshold value in the Hellinger distance that accounts for the Gaussianity validity time, reducing in that way the computational effort associated to MC simulations.
One possible application of the threshold value in the Hellinger distance is to use it as the value that triggers the splitting mechanism for a Gaussian Mixture Model (GMM) representation. The GMM will represente accurately the uncertainty distribution when a single Gaussian representation no longer holds. Finally, a practical example of GMM propagation is given using the splitting criterion defined in this work.
All the developments presented in this paper have been

Proc. 1st NEO and Debris Detection Conference, Darmstadt, Germany, 22-24 January 2019, published by the ESA Space Safety Programme Office
Ed. T. Flohrer, R. Jehn, F. Schmitz (http://neo-sst-conference.sdo.esoc.esa.int, January 2019)

implemented in Scilab, using the Celestlab toolbox [1].
The outline of the paper is structured as follows. Section 2 presents the MVN statistical tests, analyzing simulations with the selected methods : Henze-Zirkler [6] and Royston-92 [15]. Section 3 is devoted to the description of different methods of uncertainty propagation, with a special focus on the linear propagation through the State Transition Matrix, and its extension in the non-linear regime with the use of State Transition Tensor. Section 4 presents the Hellinger distance as a metric to measure the dissimilarity between two PDFs, and compares the results with respect to the statistical tests. Section 5 discusses about GMM, the splitting process and an efficient criterion to trigger it. Finally, some concluding remarks are given.

2. MULTIVARIATE NORMALITY STATISTICAL TESTS

There exists a large number of statistical tests for detecting the deviation from the MVN assumption. In [13] there are reported around 50 tests. They are usually divided in four groups as follows:

- Goodness of fit techniques, where the sample is compared to the empirical distribution function such as the Kolmogorov-Smirnov test,
- Skewness and kurtosis based techniques, that exploit the asymptotic distributions of the multivariate skewness and kurtosis to develop the test [12],
- Consistent and invariant techniques, this class of procedures proofs mathematically its *consistency* typically by using the empirical characteristic function, and
- Graphical and correlational approaches, like the quantile-quantile (Q-Q) plot [5].

In reviews and comparative analysis, there is no test that outperforms the rest uniformly, but, on the contrary, it is recommended to perform several tests to assess MVN departure. In this work, apart from graphical considerations, two statistical tests are selected : Henze-Zirkler (HZ) which is part of the group of consistent and invariant techniques and Royston-92 (R92) as a representative of goodness of fit techniques. The latter is an extension of the univariate Shapiro and Wilk test [16] that is found to be among the more powerful tests for detecting the normality breakdown in univariate cases [17].
A comprehensive set of simulations is reported in [2] comparing the performance of different tests. HZ test possesses good power [2] across the various multivariate

[1]CelestLab: CNES space mechanics toolbox for mission analysis: *https://atoms.scilab.org/toolboxes/celestlab/*

[2]The power of a statistical test is defined as the probability that it will reject a false null hypothesis. In our case, the probability that a non-MVN distribution is rejected, see Table 1.

Table 1: Error types in a statistical test.

		Null hypothesis is	
		True	False
Statistical test decision	No reject	True negative	Type II error
	Reject	Type I error	True positive (power)

distributions analyzed : T, uniform, Pearson type II and Khintchine distributions. There are two aspects in which R92 outperforms the HZ test : performance for a small sample size, and a higher power when considering multivariate normal mixtures.

2.1. Type I error rate simulations

Different simulations have been carried out to characterize the performance of both tests. This is the case of Type I error rate simulations where we want to assess that a MVN distribution will not be rejected by the statistical test. In all the simulations hereafter a significance level of 5% is used. Figure 1a shows the results for a simulation where the sample size is small, containing only 25 particles in a 3-dimensional space. In accordance to [2], HZ test is unable to achieve the nominal significance level, whether R92 test converges rapidly to 5% value. Another example is presented in Figure 1b, in which the number of particles in the sample is 1000 defined in a 6-dimensional space. In this case, both methods perform similarly and, after an initial transitory period up to 5000 MC samples, they converge to the significance level value, as expected.

2.2. Type II error rate simulations: space mechanics examples

In order to assess the power of a statistical test, one needs to draw a sample from a distribution other than the null-hypothesis. In our case, that means that we need to draw a sample from a non-MVN distribution. The methodology followed in this study is directly linked to the uncertainty propagation problem in space mechanics. An initial uncertainty distribution is drawn from a MVN distribution. In this work, the MVN distribution is defined with the position uncertainty values estimated for the Two-Lines Element (TLE) catalog. See [3] for details on the TLE catalog accuracy analysis used as example in this paper. These (rounded) values are reported in Table 2.
Two reference orbits are considered, both circular and equatorial, one in the Low Earth Orbit (LEO) at 770 km of altitude and the other in the Geostationary orbit (GEO). It is important to note that we transform those errors into

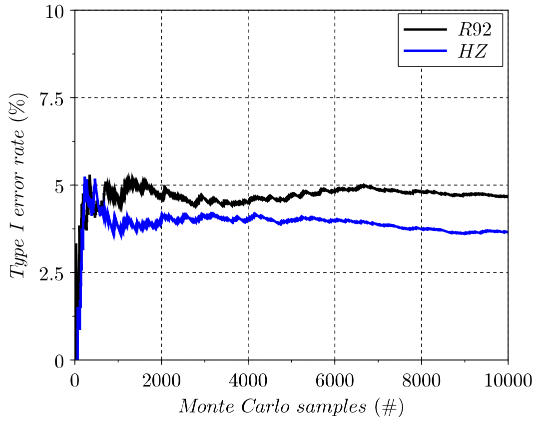

(a) Each sample is a population of 25 particles following a MVN distribution of dimension 3.

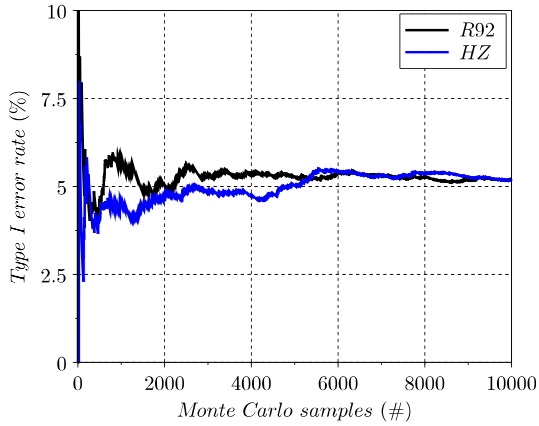

(b) Each sample is a population of 1000 particles following a MVN distribution of dimension 6.

Figure 1: Type I error rate (in percent) as a function of the number of Monte Carlo samples for R92 and HZ tests.

the Equinoctial elements space [3], with the following linearized expressions, valid for circular orbits:

$$\begin{aligned} \sigma_a &= \sigma_Q, \\ \sigma_M &= 2\,atan(\sigma_S/(2a)). \end{aligned} \tag{1}$$

Drawing the sample distribution from the equinoctial elements uncertainties induces an associated uncertainty on the velocity, in such a way that our sample distribution remains in the circular orbit regime.
Each point of the Monte Carlo sample distribution is propagated independently with unperturbed two-body dynamics. We apply the statistical tests at each time step of the Monte Carlo simulation to analyze the evolution of the normality of the distribution. The analysis of the normality departure is completed and verified with the aid of graphical methods.
The statistical test is applied to the position uncertainty distribution. For every statistical test simulation presented in this study the same configuration is used : 5000 Monte Carlo simulations containing 1000 particles (in coherence with the converged state observed in Figure 1b). In Figure 2a we can see the evolution in the case of the GEO orbit as a function of the number of orbits. At the beginning (the first two orbits) both tests remain around 95%, which corresponds to the significance level, meaning that the propagated distribution is still normal. From the second orbital period, the type II error of HZ begin to decrease until 4.5 orbital periods have passed where the value reaches zero. At that point, HZ test says the distribution is definitely no longer Gaussian. R92 test presents a similar behavior but shifted in time around 1 orbital period. Observe that the R92 test evaluates the departure from normality starting at 3.5 orbital periods, and it states that the distribution is no longer Gaussian after 5.5 orbital periods. This feature is maintained in all the simulations carried out indicating that the HZ test is more sensitive than R92 to the first signs of departure from normality.
As we have already mentioned, additional information can be obtained by graphical methods. In particular, we represent in Figure 3 the evolution of the uncertainty PDF for different time steps. It is worth noting that two orbital periods after the initial time looks like an unperturbed ellipse which is in coherence with both statistical tests that point the distribution to still be Gaussian. On the other hand, when 5 orbital periods have passed the banana-like shape appears clearly. At that moment, the type II error rate for HZ is already 0% and that of R92 test is around 20%. Both methods are indicating the non-Gaussianity of the PDF (R92 with some delay with respect to HZ results). If the application is to detect the first signs of the departure from normality, with the objective of splitting the PDF in a GMM to keep an accurate representation of the uncertainty, that point is already too late since the distribution is distorted compared to the linear (and Gaussian) propagated uncertainty. The transition phase, between the orbital periods 3 and 4, is the interval that undergoes this departure from normality. Observe that at 3 orbital periods the PDF is barely distorted and at 4 orbital periods it is evident that the PDF begins to be bent. That time corresponds to values of HZ approaching 0% and to R92 values beginning to diverge from 95%.
In the LEO case (see Figure 2b) a similar behavior is found, pointing out a departure from normality around 5 orbital periods after the initial time. Therefore, we can state that starting from a TLE-like accuracy, the orbital uncertainty expressed in Cartesian coordinates maintains the Gaussianity during 4 and 5 orbital periods in the case

[3]Equinoctial elements $(a, e_x, e_y, h_x, h_y, M)$ are defined as follows:

- Semi-major axis : a,
- Eccentricity vector $\bar{e} = (ecos(\omega+\Omega), esin(\omega+\Omega))$,
- Inclination vector : $\bar{h} = (tan(i/2)cos(\Omega), tan(i/2)sin(\Omega))$,
- Mean longitude : $\lambda_M = M + \omega + \Omega$,

where ω, Ω and M are the argument of the perigee, the right ascension of the ascending node and the mean anomaly, respectively of circular GEO and LEO orbits, respectively. Note that these values are optimistic in the sense that the dynamics only comprise two-body motion.

The degree of linearity of the dynamics of a system depends on the reference frame and type of coordinates of the state vector representation [10]. For example, cartesian coordinates applied to the elliptic motion of space objects around the Earth makes the governing equations of motion highly non-linear. However, other representations such as Equinoctial elements partly linearize the dynamics contributing to the preservation of the Gaussian assumption in the uncertainty propagation for longer time. The same Monte Carlo simulations for GEO and LEO cases are performed expressing this time the state vector in Equinoctial elements instead of Cartesian coordinates. Results of the statistic tests (see Figures 2c and 2d) show a remarkable lengthening of the time interval in which the Gaussian distribution remains valid for the uncertainty PDF representation. Indeed, in the GEO case, the validity of the Gaussian assumptions passes from several days to several years; and, in the LEO case, from several hours to several months, on the hypothesis of two-body dynamics.

3. UNCERTAINTY PROPAGATION

Uncertainty propagation is a challenging field of study, especially in orbital mechanics where dynamical systems present a highly nonlinear behavior. In [11] an extensive review of different methods for propagating uncertainties can be found. Apart from solving directly the Fokker-Planck equation, that gives the true evolution of the PDF but it is not feasible in a realistic orbital mechanics problem, the two most widely used methods are the linear propagation and the Monte Carlo simulations (see subsection 2.2 for the latter). These are opposite methods, since the former is computationally efficient but it quickly lacks of precision in nonlinear systems; and the latter provides high-precision results but at the expense of a higher computational effort. Between these two methods, there is a variety of nonlinear techniques that can be categorized in three groups:

- **Sample-based methods**: This type of techniques, that comprises also the Monte Carlo simulations, generates a set of samples representing the initial uncertainty, propagates these samples individually, and then reconstructs the propagated uncertainty. In that way, the dynamics (propagator) is considered as a black box, and we refer to this kind of methods as *non-intrusive*. Methods, others than MC simulations, strives for choosing efficiently the samples in order to reduce the computational effort. Unscented transform [9] and Polynomial Chaos Expansion [8] are examples of these techniques.

- **Dynamics-based methods** : These methods approximate the dynamics around the nominal trajectory based on a Taylor series expansion, and used this *simplified* dynamics in the propagation of uncertainties. The Taylor series can be built up either with the computation of high-order partial derivatives forming State Transition Tensors (the nonlinear analogy to state transition matrix) [14, 4], or by means of Differential Algebra techniques [18].

- **PDF-based method** : This approach aims to represent the PDF in such a way that the effects of nonlinearity in dynamics are reduced in the propagation. This is the idea of Gaussian Mixture Models [1]. A Gaussian mixture is a weighted sum of Gaussian density function that can represent any PDF as accurate as desired by increasing the number of Gaussian kernels in the mixture. Propagation of each individual Gaussian PDF is less affected to errors due to nonlinearities, and the overall GMM function can represent the true evolution of the uncertainty with high-accuracy.

Table 2: Initial orbit and position uncertainty.

Orbital regime	Semi-major axis (km)	Radial σ_Q (m)	Along-track σ_S (m)
LEO	7148.1	100	470
GEO	42164.5	360	430

Propagation schemes used within this study are further detailed hereafter.

3.1. Linear Propagation - State Transition Matrix

Being $\boldsymbol{x}$ the state vector of a space object that undergoes a dynamical evolution described by the governing equation:

$$\dot{\boldsymbol{x}} = \vec{f}(\boldsymbol{x}), \quad (2)$$

where dot denotes derivative with respect to time. The evolution of a small error $\delta\boldsymbol{x}$ in the state vector can be approximated to the first order (linearization) as :

$$\dot{\boldsymbol{x}} + \delta\dot{\boldsymbol{x}} = \vec{f}(\boldsymbol{x} + \delta\boldsymbol{x}) \simeq \vec{f}(\boldsymbol{x}) + \frac{\partial \vec{f}(\boldsymbol{x})}{\partial \boldsymbol{x}}\delta\boldsymbol{x}. \quad (3)$$

Using Eq. 2, this expression is simplified to:

$$\delta\dot{\boldsymbol{x}} \simeq \frac{\partial \vec{f}(\boldsymbol{x})}{\partial \boldsymbol{x}}\delta\boldsymbol{x} = \boldsymbol{F}\delta\boldsymbol{x}. \quad (4)$$

Being the small error a quantity dependent on time ($\delta\boldsymbol{x} = \delta\boldsymbol{x}(t)$), we can approximate it with a Taylor series expansion in time:

$$\delta\boldsymbol{x} \simeq \delta\boldsymbol{x}_0 + \delta\dot{\boldsymbol{x}}_0(t - t_0) \simeq \delta\boldsymbol{x}_0 + \boldsymbol{F}\delta\boldsymbol{x}_0(t - t_0), \quad (5)$$

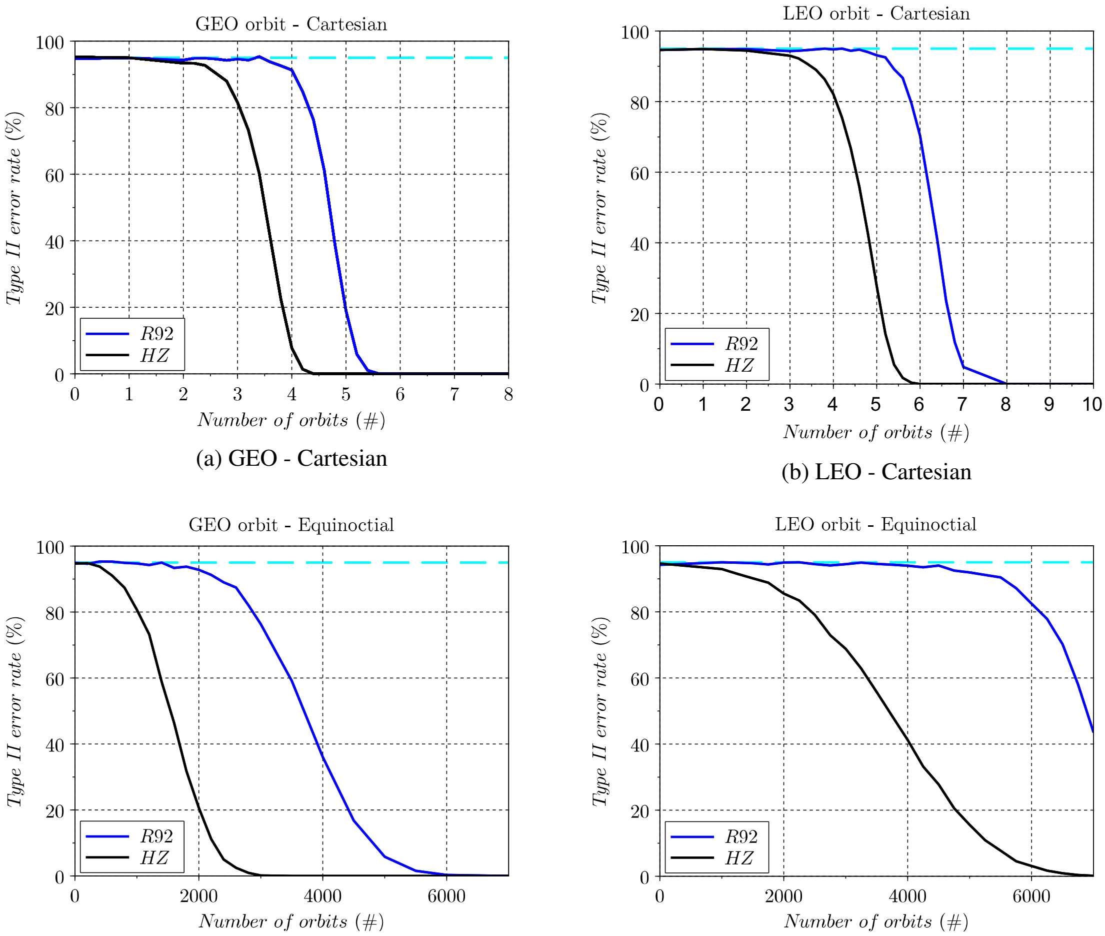

(a) GEO - Cartesian

(b) LEO - Cartesian

(c) GEO - Equinoctial

(d) LEO - Equinoctial

Figure 2: Type II error rate (in percent) as a function of the number of orbits. R92 (blue line) and HZ (black line) statistical tests results are displayed. Dashed light blue line represents the significance level for a MVN distribution. The initial orbital uncertainty associated to each orbit is defined in Table 2

where $\delta \boldsymbol{x}_0$ corresponds to the small error at the initial time, t_0. Then, we arrive to a linear matricial expression relating the small error at two different times:

$$\delta \boldsymbol{x} \simeq (\boldsymbol{I} + \boldsymbol{F}(t - t_0))\delta \boldsymbol{x}_0 = \Phi \delta \boldsymbol{x}_0, \tag{6}$$

where Φ is the State Transition Matrix. Considering a two-body dynamical model expressed in equinoctial elements, $\boldsymbol{F}$ is a 6x6 matrix with all elements zero except $\boldsymbol{F}_{61} = -3\mu^{1/2}/(2a^{5/2})$.

If we consider an unbiased initial perturbation $\delta \boldsymbol{x}_0$ following a MVN distribution of covariance P_0, we can define the linear evolution of the uncertainty with the evolution of the mean and covariance:

- Mean : $m = E\left[\delta \boldsymbol{x}\right] = \Phi E\left[\delta \boldsymbol{x}_0\right] = 0$, since $E\left[\delta \boldsymbol{x}_0\right] \equiv 0$ from the unbiased hypothesis.

- Covariance : $P = E\left[\delta \boldsymbol{x}\ \delta \boldsymbol{x}^T\right] - mm^T = \Phi E\left[\delta \boldsymbol{x}_0\ \delta \boldsymbol{x}_0^T\right] \Phi^T = \Phi P_0 \Phi^T$

3.2. Nonlinear Propagation - State Transition Tensor

This nonlinear propagation is the extension of the STM approach when considering higher order terms of the Taylor series expansion. We will consider hereafter up to the second term of the expansion, but generalization to higher order terms is straightforward. Einstein notation is used for convenience. The dynamics of small perturbations (Eq. 4) becomes:

$$\delta \dot{x}_i \simeq \frac{\partial f_i}{\partial x_{k_1}} \delta x_{k_1} + \frac{1}{2} \frac{\partial^2 f_i}{\partial x_{k_1} \partial x_{k_2}} \delta x_{k_1} \delta x_{k_2} = F_{i,k_1} \delta x_{k_1} + \frac{1}{2} F_{i,k_1 k_2} \delta x_{k_1} \delta x_{k_2}, \tag{7}$$

where the superspript (2) refers to second order derivation. The mapping of perturbation from initial to final

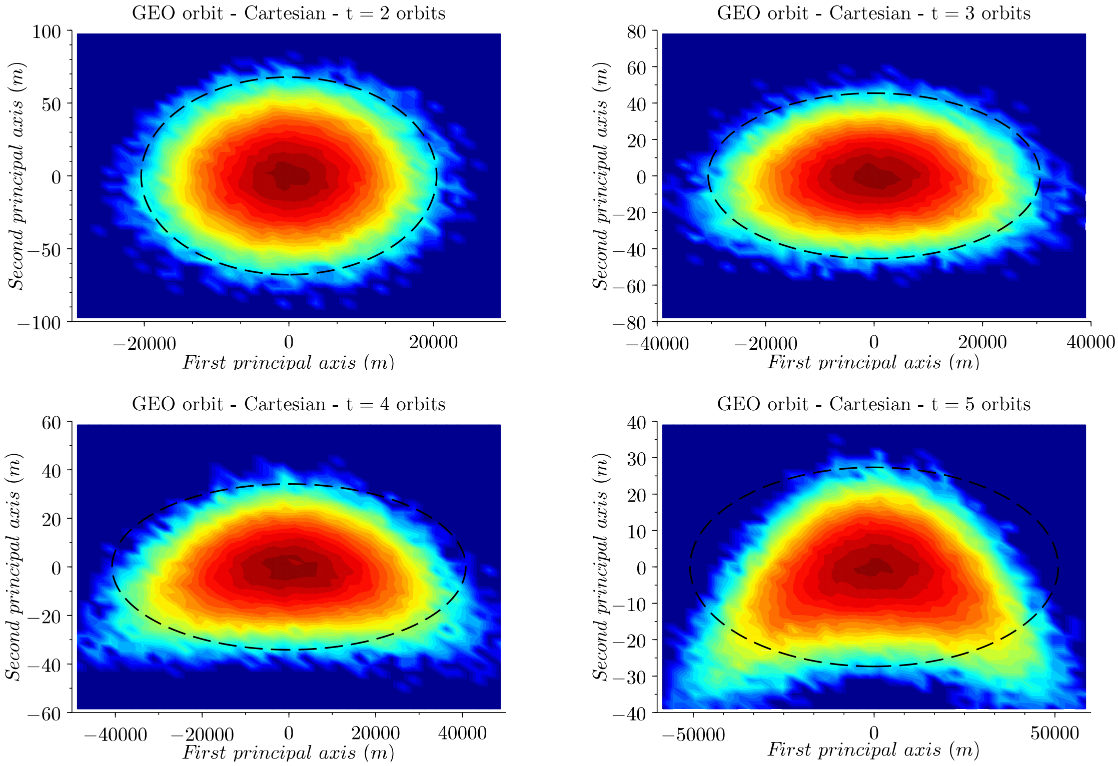

Figure 3: Evolution of the position uncertainty in the equatorial plane. The axis are aligned with the principal axis of the linearly propagated covariance. Probability density is computed from 200 Monte Carlo simulations containing 500 particles. Dashed black line corresponds to the 3-sigma value ellipse of the position covariance.

time (Eq. 6) is modified to:

$$\delta x_i \simeq \Phi_{i,k_1}\delta x^0_{k_1} + \frac{1}{2}\Phi_{i,k_1k_2}\delta x^0_{k_1}\delta x^0_{k_2} = \sum_{p=1}^{2}\frac{1}{p!}\Phi_{i,k_1\ldots k_p}\delta x^0_{k_1}\ldots\delta x^0_{k_p} \quad (8)$$

where the superscript (0) refers to initial conditions and $\Phi_{i,k_1k_2} \equiv F_{i,k_1k_2}$ is a tensor of second order that can be represented, in our problem, with a 6x6x6 hypermatrix. For two-body dynamics expressed in Equinoctial elements, this hypermatrix is completely empty except for one term : $\Phi_{611} = 15\mu^{1/2}/(4a^{7/2})$. Generalization for higher order terms of the two-body dynamics gives:

$$\Phi_{6,\underbrace{1,\ldots,1}_{p\text{ times}}} = (-1)^p\frac{(2p+2)!}{2^{2p+1}(p+1)!}\frac{\mu^{1/2}}{a^{(3+2p)/2}} \quad (9)$$

The nonlinear evolution, up to second order, of the initial perturbation $\delta\boldsymbol{x}_0 = \mathcal{N}\left(0, P^0\right)$ is given by:

$$m_i = \sum_{p=1}^{2}\frac{1}{p!}\Phi_{i,k_1\ldots k_p}E\left[\delta x^0_{k_1}\ldots\delta x^0_{k_p}\right] = \frac{1}{2}\Phi_{i,k_1k_2}P^0_{k_1k_2}. \quad (10)$$

$$\begin{aligned} P_{ij} =& \sum_{p=1}^{2}\sum_{q=1}^{2}\frac{1}{p!q!}\Phi_{i,k_1\ldots k_p}\Phi_{j,l_1\ldots l_q} \\ & E\left[\delta x^0_{k_1}\ldots\delta x^0_{k_p}\ \delta x^0_{l_1}\ldots\delta x^0_{l_q}\right] - m_i m_j \\ =&\Phi_{i,k_1}\Phi_{j,l_1}P^0_{k_1l_1} - m_i m_j + \\ & \frac{1}{4}\Phi_{i,k_1k_2}\Phi_{j,l_1l_2}[P^0_{k_1k_2}P^0_{l_1l_2} + P^0_{k_1l_1}P^0_{k_2l_2} + \\ & P^0_{k_1l_2}P^0_{k_2l_1}] \end{aligned} \quad (11)$$

Note that, in contrast with the linear evolution, there is a non-zero mean, that is to say, the mean value of the perturbation is deviated with respect to the reference trajectory.

4. SIMILARITY METRIC BETWEEN DISTRIBUTIONS

In probability theory, there are different functions to measure the similarity or closeness between two probability distribution functions. On one hand, we have the distance metrics, d, that are measures satisfying four conditions :

1. non-negativity ($d(p,q) \geq 0$, where p and q are the two PDFs),
2. identity of indiscernibles ($d(p,q) = 0 \rightarrow p = q$),

3. symmetry ($d(p,q) = d(q,p)$) and
4. the triangle inequality ($d(p,r) \leq d(p,q) + d(q,r)$,

where r is a third PDF. On the other hand, we have weaker notions of the distance metrics, as, for example, the divergences that only satisfy the first two conditions defining a positive-definite function. Examples of the latter are the Kullback-Leibler divergence or, its generalization, the Rényi divergence [20]. In this study, the Hellinger distance metric is used.

4.1. Hellinger distance

The Hellinger distance, in a given space state Υ, is defined as follows:

$$d_H(p,q) = \left[\frac{1}{2}\int_{\Upsilon}(p(x)^{\frac{1}{2}} - q(x)^{\frac{1}{2}})^2 dx\right]^{\frac{1}{2}}. \tag{12}$$

The above expression can be simplified to:

$$d_H(p,q) = \left[1 - \int_{\Upsilon} p(x)^{\frac{1}{2}} q(x)^{\frac{1}{2}} dx\right]^{\frac{1}{2}} = [1 - BC]^{\frac{1}{2}}, \tag{13}$$

where BC is the Bhattacharyya coefficient. In the case that both p and q are MVN distributions ($p = \mathcal{N}(x; m_p, P_p)$ and $q = \mathcal{N}(x; m_q, P_q)$), the Bhattacharyya coefficient gets reduced to:

$$BC = \frac{|P_p|^{\frac{1}{4}}|P_q|^{\frac{1}{4}}}{|\bar{P}|^{\frac{1}{2}}} \exp\left(-\frac{1}{8}\Delta m^T \bar{P}^{-1}\Delta m\right), \tag{14}$$

where $\bar{P} = (P_p + P_q)/2$, $\Delta m = m_p - m_q$. This distance is bounded and it can take values in the range $0 \leq d_H \leq 1$, where the value $d_H = 0$ indicates two identical distributions and, on the contrary, the value $d_H = 1$ points to two completely dissimilar distributions. One of the interests for using this distance is its scale-invariant nature. This will facilitate the choice of a threshold value representing the time when nonlinear terms become non-negligible in the uncertainty propagation (see Section 2.2).

4.2. Comparison between Hellinger distance and statistical tests for MVN

In this section we are going to compare the evolution of the Hellinger distance, computed from the uncertainties propagated linearly and non-linearly with the STTs, and the evolution of the statistical tests, computed from the Monte Carlo simulations. The former is a rapid computation from the analytical expressions presented in Section 3 for the two-body dynamics, and the latter is a time expensive computation but applied to the most realistic representation of the uncertainty PDF which is the Monte Carlo sample (see Section 2). The objective is to derive a relationship that allows us to confidently use the Hellinger distance as a measure of Gaussianity breakdown.
Figure 4 shows the statistical tests values as a function of the square of the Hellinger distance. This is possible as both functions are monotonic with respect to time. Different initial uncertainties in position have been assessed. The index in the cases reported in Figure 4 refer to these different initial uncertainty factors: an index "11" means that the same values as in Table 2 have been used (so the same case of Figure 2c), and index "12" means that the same uncertainty in the radial position is used but the double for the along-track uncertainty, and so on. It is worth noting the remarkable similarity of the results obtained for the different cases. Thus, we can state that there is a clear relationship between the normality breakdown observed in the Monte Carlo simulations, and the analytical analysis where the importance of the non-linear terms contained in the State Transition Tensor is assessed via the Hellinger distance. In other words, the non-linearity effects captured by the Hellinger distance represent a high-fidelity measure of the departure from normality detected in the MC simulations. In this way, it is possible to use this Hellinger distance instead of MC simulations for estimating the departure from normality, with the advantage of a considerable gain in computational time. With the help of graphical methods, the value $d_H^2 = 0.005$ is set hereafter as the threshold value for the departure from normality.
Having set the threshold value, we can rapidly explore different cases of initial uncertainty to perform a parametric study on the departure from Gaussianity. Figure 5 presents such a study, where the initial uncertainties in both directions are varied between 300 m and 3 km. We recover the value of the case presented in Figure 2c as a point between the level curves of 2000 and 3000 orbital periods. In two-body dynamics expressed in Equinoctial elements, the main driver of non-linearity comes from the evolution of the mean anomaly with respect to deviations in the semi-major axis, that is to say, the position uncertainty on the radial direction drives the non-linearity, and, hence, the departure from normality. This fact is observed in Figure 5 as the constant decrease of the orbital periods before Gaussianity breakdown when we move rightwards (increasing σ_a). One passes from around 24000 orbital periods with $(\sigma_Q, \sigma_S) = (300\,\mathrm{m}, 300\,\mathrm{m})$ to 24 orbital periods with $(\sigma_Q, \sigma_S) = (3000\,\mathrm{m}, 300\,\mathrm{m})$, that is to say, a decrease of three order of magnitudes in the Gaussianity validity time caused by an increase of one order of magnitude in the radial direction uncertainty.
It is worth noting that the level curves in Figure 5 are such that an increase of initial uncertainty in an arbitrary direction does not lead invariably to a shorter validity time of the Gaussian assumption. Observe that we can follow a level curve, which is line of constant time for Gaussianity breakdown, by increasing the position uncertainty in both directions. In other words, the size of the uncertainty is not the only factor that plays a role in the evolution of the normality of the distribution but also the *aspect ratio* of the associated ellipse.

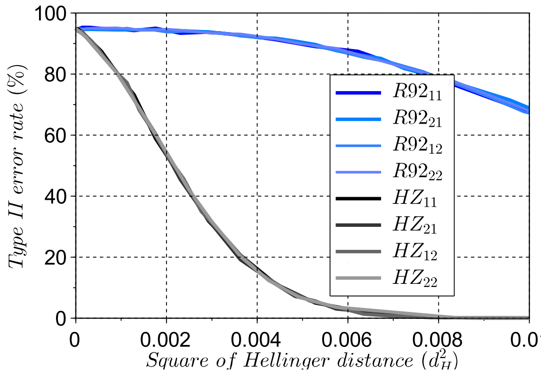

Figure 4: Type II error rate (in percent) as a function of the square of the Hellinger distance computed from linear Vs STT propagation. R92 (degradation of blue lines) and HZ (degradation of gray lines) are displayed.

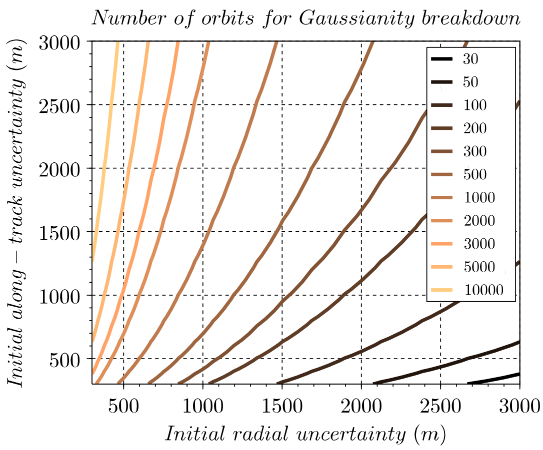

Figure 5: Contour plot in the GEO case representing the number of orbital periods before the departure from normality as a function of the initial position uncertainties in the radial and along-track directions.

5. GAUSSIAN MIXTURE MODEL

In the propagation process, when the uncertainty distribution begins to depart from normality, another PDF other than a single MVN distribution shall be used to ensure an accurate representation. One candidate, which is a direct extension of the Gaussian distribution, is the Gaussian mixture model. A GMM is a weighted sum of single MVN components:

$$p(\boldsymbol{x}) = \sum_{i=1}^{n} w_i \mathcal{N}\left(\boldsymbol{x}; \boldsymbol{m}_i, \boldsymbol{P}_i\right), \tag{15}$$

where n is the number of components of the mixture and w_i the weight of each component. These weights shall be all positive and sum to one in order Eq. 15 to be a valid PDF. For a sufficient number of components, we can accurately approximate many complex distributions.

Table 3: Five-Component Splitting Library.

i	w_i	μ_i	σ
1	0.076322	-1.689973	0.442256
2	0.247442	-0.800928	0.442256
3	0.352473	0.0	0.442256
4	0.247442	0.800928	0.442256
5	0.076322	1.689973	0.442256

The procedure that converts a single MVN into a Gaussian mixture is called splitting. This splitting mechanism should be integrated into the uncertainty propagation scheme and, therefore, we need a simple and efficient splitting criterion that monitors the validity of the Gaussian assumption for each MVN component.

5.1. Splitting methodology

The splitting of a MVN distribution is simplified if we make use of the solution of the univariate standard normal distribution. The univariate case is reduced to a constrained nonlinear optimization problem that we do not need to solve every time but only once. Thus, we can speak of *splitting libraries* which are the solutions of this optimization problem. In this work, we use a splitting library [1] that divides the Gaussian distribution into five components (see Table 3). The number of components in the Gaussian mixture is dependent on the desired accuracy of the sum approximation [7], the use of five components in this work is only an example.
The multivariate case can be solved in several ways depending on the direction(s) of splitting. We are going to apply the splitting in one direction corresponding to the direction of maximal uncertainty (the eigenvector associated the largest eigenvalue of the covariance matrix). The procedure for splitting the multivariate distribution $\mathcal{N}\left(x; m^0, P^0\right)$ is as follows (see [1] for further details):

1. $P^0 = V\Lambda V^T$, where V the eigenvector matrix and Λ the eigenvalue diagonal matrix,

2. $m_i = m^0 + \sqrt{\lambda_k}\mu_i v_k$, where m_i is the mean of the ith component, λ_k the largest eigenvalue, v_k the eigenvector associated to λ_k and μ_i is taken from the splitting library (see Table 3),

3. $\Lambda_i = diag\left\{\lambda_1, \ldots, \sigma^2\lambda_k, \ldots, \lambda_n\right\}$, where σ is taken from the splitting library,

4. $P_i = V\Lambda_i V^T$, where P_i. is the covariance matrix of the *ith* component (see Eq. 15).

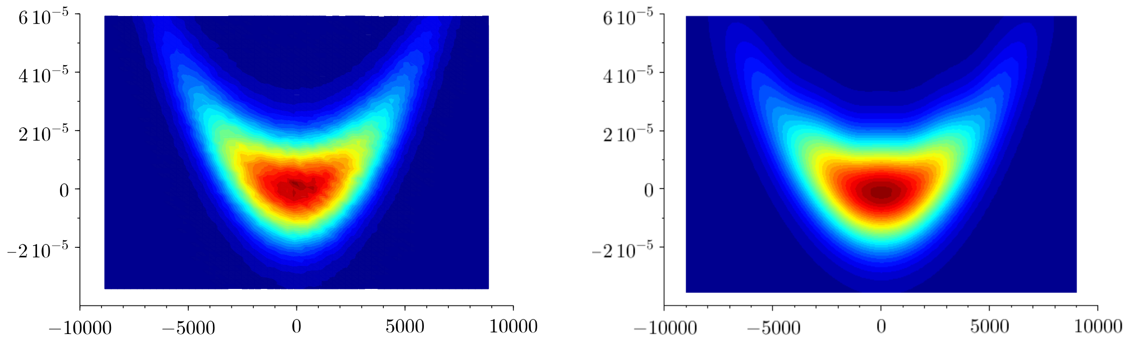

(a) Monte Carlo simulation : 100 samples with a population of 15000 particles each sample

(b) Propagated Gaussian mixture distribution with 5 components split at $t = 39.5$ orbits.

Figure 6: Uncertainty distribution after 200 orbital periods propagation. PDFs are plotted in the principal axis of the linearly propagated covariance in the semi-major axis - mean anomaly plane.

5.2. Splitting criterion

The splitting criterion that we propose is to monitor the evolution of the Hellinger distance between the uncertainty distributions propagated linearly and non-linearly with the STTs and to trigger the splitting mechanism when that distance equals the threshold value $d_H^2 = 0.005$. This is applicable to the initial Gaussian distribution as well as to all the components of the GMM.
A simulation is performed with the GEO orbit defined in Table 2. The initial position uncertainty corresponds to a 1-sigma value in the radial direction of 3000 m and 500 m for the along-track direction. With these values, the Hellinger distance reaches the threshold value after, approximately, 39.5 orbital periods. Observe in Figure 5 that this initial uncertainty lies between the iso-lines of 30 and 50 orbital periods. The Gaussian distribution is then split into a GMM of 5 components, and the propagation of uncertainty resumes until reaching 200 orbital periods. In the interval where the distribution is described by the GMM, none of the components arrive to the threshold value in its own Hellinger distance. The propagated uncertainty distribution can then be compared with the results of a Monte Carlo simulation. Such a comparison is done in Figure 6. The agreement between distributions is remarkable, both in size than in shape.
In order to assess the gain in performance in the uncertainty propagation with the proposed approach, we compare the computational time required for the simulations of Figure 6. All computations are performed on a laptop, 2.50 GHz Intel® Core™ i5-7200U and 8 GB RAM. The Monte Carlo simulation takes around 7 mn and 30 s (450 s), and the Gaussian Mixture Model with linear propagation and splitting based on the Hellinger distance needs 15 s to perform the simulations. That is to say, in this example, the proposed approach is 30 times faster than a MC simulation.

6. CONCLUSIONS

The Gaussianity validity time has been assessed in the frame of orbital uncertainty propagation by means of different multivariate normal statistical tests. In particular, Henze-Zirkler and Royston-92 tests have been used along with graphical methods. Monte Carlo simulations for two orbital regimes, GEO and circular LEO, have been performed in the case of an initial position uncertainty in accordance with the expected accuracy of the Two-Line Element catalogue of resident space objects. The importance of the linearity of the governing equations of motion for holding the Gaussianity assumption a longer time has been evaluated by choosing a judicious coordinates system representation. With unperturbed two-body dynamics, Equinoctial elements representation leads the Gaussianity validity time around three order of times longer than in the case of Cartesian coordinates.
Linearity of the system is assessed by comparing the uncertainty distribution propagated linearly with the State Transition Matrix and non-linearly with the State Transition Tensor of second order. This comparison is performed by means of a distance metric, the Hellinger distance, which is scale-invariant. For different test cases, a clear relationship between this Hellinger distance and the results of the statistical tests is observed. Hence, the Hellinger distance that measures the non-linearity with the State Transition Tensor can also be used as a measure of the departure from normality. A threshold is set on the Hellinger distance to define the time of Gaussianity breakdown. This threshold value can be used as the criterion to split a single Gaussian distribution into a Gaussian Mixture Model.
A simulation of uncertainty propagation is carried out with a Gaussian Mixture Model including the splitting mechanism triggered by the Hellinger distance threshold. A comparison with the equivalent Monte Carlo simulation is performed showing good agreement. Therefore, our work shows that, for the unperturbed two-body

motion dynamics, the Hellinger distance based on the non-linearities captured by the STT can be used instead of the MC to detect the departure from Gaussianity.

REFERENCES

1. DeMars, K. J., Bishop, R. H., and Jah, M. K. (2013). Entropy-based approach for uncertainty propagation of nonlinear dynamical systems, *Journal of Guidance, Control, and Dynamics*, **36**(4), 1047-1057.

2. Farrell, P. J., Salibian-Barrera, M., and Naczk, K. (2007). On tests for multivariate normality and associated simulation studies, *Journal of statistical computation and simulation*, **77**(12), 1065-1080.

3. Flohrer, T., Krag, H. and Klinkrad, H. (2008). Assessment and Categorization of TLE Orbit Errors for the US SSN Catalogue. In Proc. Advanced Maui Optical and Space Surveillance Technologies Conference, 17 - 19 September 2008, Wailea, Maui, USA.

4. Fujimoto, K., Scheeres, D. J., and Alfriend, K. T. (2012). Analytical nonlinear propagation of uncertainty in the two-body problem, *Journal of Guidance, Control, and Dynamics*, **35**(2), 497-509.

5. Healy, M. (1968). Multivariate normal plotting, *Applied Statistics*, **17**(2), 157–161

6. Henze, N., and Zirkler, B. (1990). A class of invariant consistent tests for multivariate normality, *Communications in Statistics - Theory and Methods*, **19**(10), 3595-3617.

7. Horwood, J. T., Aragon, N. D., and Poore, A. B. (2011). Gaussian sum filters for space surveillance: theory and simulations, *Journal of Guidance, Control, and Dynamics*, **34**(6), 1839-1851.

8. Jones, B. A., Doostan, A., and Born, G. H. (2013). Nonlinear propagation of orbit uncertainty using non-intrusive polynomial chaos. *Journal of Guidance, Control, and Dynamics*, **36**(2), 430-444.

9. Julier, S. J., and Uhlmann, J. K. (2004). Unscented filtering and nonlinear estimation, *Proceedings of the IEEE*, **92**(3), 401-422.

10. Junkins, J. L., and Singla, P. (2003). How nonlinear is it? A tutorial on nonlinearity of orbit and attitude dynamics. *Advances in the Astronautical Sciences*, **115**(SUPPL.), 1-45.

11. Luo, Y-Z, and Yang, Z. (2017). A review of uncertainty propagation in orbital mechanics, *Progress in Aerospace Sciences*, **89** 23-39

12. Mardia, K. V. (1970). Measures of multivariate skewness and kurtosis with applications, *Biometrika*, **57**(3), 519-530.

13. Mecklin, C. J., and Mundfrom, D. J. (2005). A Monte Carlo comparison of the Type I and Type II error rates of tests of multivariate normality, *Journal of Statistical Computation and Simulation*, **75**(2), 93-107.

14. Park, R. S., and Scheeres, D. J. (2006). Nonlinear mapping of Gaussian statistics: theory and applications to spacecraft trajectory design, *Journal of guidance, Control, and Dynamics*, **29**(6), 1367-1375.

15. Royston, J.P., (1992). Approximating the Shapiro-Wilk W-Test for non-normality, *Statistics and Computing*, **2**, 117-119.

16. Shapiro, S. S., and Wilk, M. B. (1965). An analysis of variance test for normality (complete samples), *Biometrika*, **52**(3/4), 591-611.

17. Srivastava, M. S., and Hui, T. K. (1987). On assessing multivariate normality based on Shapiro-Wilk W statistic, *Statistics and Probability Letters*, **5**(1), 15-18.

18. Valli, M., Armellin, R., Di Lizia, P., and Lavagna, M. R. (2012). Nonlinear mapping of uncertainties in celestial mechanics. *Journal of Guidance, Control, and Dynamics*, **36**(1), 48-63.

19. Van der Vaart, A. W. (2000). *Asymptotic statistics*, Cambridge university press, Vol. 3.

20. Van Erven, T., and Harremos, P. (2014). Rényi divergence and Kullback-Leibler divergence. *IEEE Transactions on Information Theory*, **60**(7), 3797-3820.